Contents lists available at ScienceDirect

Materials Today Nano

Two-dimensional nanomaterials for novel piezotronics and piezophototronics

P. Lin [a], C. Pan [a, **], Z.L. Wang [a, b, c, *]

[a] CAS Center for Excellence in Nanoscience, Beijing Key Laboratory of Micro-nano Energy and Sensor, Beijing Institute of Nanoenergy and Nanosystems, Chinese Academy of Sciences, Beijing 100083, PR China
[b] School of Nanoscience and Technology, University of Chinese Academy of Sciences, Beijing 100049, PR China
[c] School of Material Science and Engineering, Georgia Institute of Technology, Atlanta, Georgia 30332, United States

ARTICLE INFO

ABSTRACT

Because of the novel properties owing to two-dimensional (2D) confinement, research on 2D nanomaterials has become one of the leading topics in condensed matter physics and materials science. From the viewpoint of crystallography, the 2D morphology embodies spontaneous breakdown of three-dimensional symmetry, which means that the inversion symmetry preserved in some bulk materials can be broken in their corresponding 2D ones, possibly resulting in intrinsic piezoelectric property. Such 2D materials in conjunction with their semiconductor properties are good candidates for novel ultrathin piezotronics and piezophototronics. In one hand, the 2D piezoelectric materials are easy to integrate with the state-of-the-art semiconductor process and conventional electronic technologies. On the other hand, the possible combination of piezoelectricity with other unusual properties in 2D materials such as ferromagnetism or topological insulator may give birth to new physics and innovative devices design for novel applications. Here, we present an overview of recent breakthroughs in 2D piezotronics and piezophototronics, covering from the fundamental principles to their vast applications in energy harvesting and adaptive electronics/optoelectronics. Considering the potential scientific and device developments, we conclude with an in-depth discussion of possible future directions in this active research field.

© 2018 Elsevier Ltd. All rights reserved.

1. Introduction

Piezoelectric effect is unique in a way that couples mechanical stimulation with electronic output and has found a wide range of applications in electromechanical sensors, actuators, and energy converters since its discovery in 1880. From then on, the most widely investigated traditional piezoelectric materials mainly include a mass of inorganic perovskite ceramic crystals (e.g. lead zirconate titanate) and organic polymers (e.g. poly (vinylidene fluoride)) [1—4]. Owing to the intrinsic insulation nature of these materials, the coupling research between piezoelectric-induced polarization and electronic/optoelectronic processes had consequently long been ignored until the discovery of piezoelectric nanogenerators (NGs) using ZnO nanowire arrays by Wang in 2006 [5]. It verifies that the piezoelectricity can be well preserved in

semiconductors even under the existence of moderate free charge carriers, opening up a new frontier for microenergy/nanoenergy and self-powered system research [6—9]. By taking advantage of the multiple functionalities offered by piezoelectric semiconductors, Wang proposed the groundbreaking device concepts of piezotronics and piezophototronics in 2007 and 2010, respectively [10—14]. From this new physical principle, unprecedented device technologies have been developed with vast potential applications in active sensors, human-complementary metal oxide semiconductor (CMOS) interfacing, logic computation, and nanorobotics [15—19]. Among these piezoelectric semiconductors, the wurtzite-structured ZnO, GaN, and CdS with morphology of one-dimensional (1D) nanowires and nanobelts are the most often investigated [20—24]. Afterward, the existence of piezoelectric effect in semiconductor materials of other crystal structure has also been demonstrated, which shows the universality of piezoelectric semiconductors and greatly increases the selectivity of materials for piezotronics and piezophototronics. After more than one decade of intensive efforts, the coupling research between piezopolarization and semiconductor behaviors has logically developed into a

* Corresponding author. School of Material Science and Engineering, Georgia Institute of Technology, Atlanta, GA 30332, United States.
** Corresponding author.
E-mail addresses: cfpan@binn.cas.cn (C. Pan), zhong.wang@mse.gatech.edu (Z.L. Wang).

large field of its own and still remains one of the most active research areas for the third-generation semiconductors.

Since the first measurement of single atomic layer graphite (graphene) in 2004, the research on atomically thin crystals has exploded, and the library of two-dimensional (2D) materials has greatly expanded, including conductors, semiconductors with varying bandgaps (e.g. MoS_2 and WSe_2), and insulators (e.g. h-BN) [25—28]. Owing to the 2D confinement, these materials display unique electronic, optical, and mechanical properties that are unattainable in their bulk counterparts [29—31]. For instance, the dangling bond-free surface of atomic layer allows stacking integration of disparate 2D materials without the constraint of lattice matching to create artificial van der Waals (vdWs) heterostructures or superlattices, giving rise to a new platform for exploring new physics at the atomic scale [32,33]. In addition, from the point of crystallography, the reduced 2D dimensionality embodies spontaneous breakdown of three-dimensional (3D) symmetry. Consequently, some non-piezoelectric bulk materials may become intrinsically piezoelectric when thinned to single atomic layer. This extends the concept of piezotronics and piezophototronics into a new arena of 2D materials, which may well bring further scientific and device developments. First, compared with the 1D and 3D morphology, the crystal structure of 2D materials is simpler. This facilitates the research of structure-property relationship in piezoelectricity from the first-principles simulation, which could advance our fundamental understanding of this old physical effect. Moreover, the possible combination of piezotronic/piezophototronic effects with other exotic properties in 2D materials such as ferromagnetism, topological insulators, or quantum spin Hall effect are still far from being fully explored. Furthermore, the 2D materials are easy to fully integrate with the standard semiconductor process and well-developed conventional electronic technologies, which may enable the array integration of piezotronics/piezophototronics and accelerate their process of practicality.

In this review, we will summarize the recent advances in piezotronics/piezophototronics fabricated using novel 2D nanomaterials. A brief discussion on the fundamental principles of piezotronic and piezophototronic effect is first introduced, followed by the recent studies of piezoelectricity in 2D nanomaterials. Then, theoretical and experimental investigation of 2D piezotronics and piezophototronics are highlighted, emphasizing their potential applications in energy harvesting and adaptive electronics/optoelectronics. In addition, we propose several 2D materials systems that can be adopted for piezotronics/piezophototronics. Finally, we offer our forward-looking perspectives on the future challenges and possible scientific breakthroughs in this burgeoning research field.

2. Fundamental principles of piezotronic and piezophototronic effects

Compared with the conventional electronics (e.g. field-effect transistors) that rely on the electrostatic coupling between electric field induced by gate voltage and conductive channel, the piezotronics and piezophototronics represent a totally new semiconductor-device category through tailoring the interfacial property. For piezoelectric semiconductors with moderate charge carrier density, strain-induced non-mobile piezopolarization charges at the vicinity of contact or interface can effectively modulate the interfacial energy-band profile and hence the carrier transport across the junction, and this is the basis of piezotronic effect [34,35]. This novel coupling mode between piezoelectricity and electronic transport has inspired the inventions of many innovative electronic devices, such as flexible strain/stress sensors, strain-gated logic units, and nanorobotics [36—38]. The

piezophototronic effect is a result of three-way coupling between piezoelectricity, photonic excitation, and semiconductor transport. By using the strain-induced piezopotential, the electro-optical processes including carrier generation, transport, separation, and/or recombination at the metal-semiconductor Schottky contact or p-n junction can be deliberately controlled [39,40]. Based on this fundamental principle, the piezophototronic-enhanced optoelectronics involving photosensors, light-emitting diodes (LEDs), solar cells, and even the photoelectrochemical devices have been widely demonstrated [41—47]. In this section, we will take the Schottky contact and p-n junction as an example to qualitatively illustrate the piezotronic and piezophototronic effects; more detailed numerical simulations can be found in other papers [48—52]. For Schottky contact formed by n-type piezoelectric semiconductor and metal, strain-induced negative piezoelectric polarization charges at the interface will further deplete the major electron carriers in a semiconductor, leading to increased interfacial Schottky barrier height (SBH) and thus the upward bending of energy band (Fig. 1a). Alternatively, the positive piezoelectric polarization charges can attract the free electrons, consequently the barrier interface becomes less depleted and energy-band bends downward (Fig. 1b). It is worth mentioning that because of the ultra-high concentration of electrons in metal, the impact of piezoelectric potential on metal side could be ignored. Nevertheless, for p-n heterojunction formed by p-type non-piezoelectric semiconductor and n-type piezoelectric semiconductor with similar and moderate doping concentration, the interfacial piezopolarization charges can influence the band tilting in both materials. Generally, the strain-induced negative polarization charges lead to upward bending of interfacial energy bands; therefore, the depletion width in n- and p-type semiconductor increases and decreases, respectively (Fig. 1c). In this case, the whole depletion region shifts toward the n-type side. Instead, the positive polarization charges decrease the depletion width in n-type semiconductor and the whole depletion region shifts toward the p-type side (Fig. 1d). Moreover, if the density of positive piezopolarization charges are so large that it completely inverts the band tilting direction at the n-type side, the local deformation of band structure will create a channel for trapping electrons. For LEDs, the presence of such electron traps at the interface will increase the recombination possibility of electron-hole pairs, leading to enhanced electro-optical conversion efficiency [16,53]. In brief, the piezotronic and piezophototronic devices are fabricated by using piezopotential as a 'gate' to modulate the electronic and optoelectronic process in semiconductor devices. This interdisciplinary field not only brings new physics to classic semiconductor theory but also opens up a new route to the artificial design of semiconductor interface with mechanical stimulation for enhanced electronics/optoelectronics and other novel applications.

3. Piezoelectricity in 2D nanomaterials

With the advance of materials synthesis at the molecular level, the piezoelectricity in novel 2D materials is attracting more and more attention [54,55]. Based on crystallography, it is well known that all non-centrosymmetric point groups (except the cubic class 432) show piezoelectric effect. Compared with their bulk counterparts, the origin of piezoelectricity in novel 2D materials could be generally separated into three distinct categories. First, the conventional 3D piezoelectric materials still preserve the piezoelectricity when thinning down to several nanometers, such as the hexagonal CdS and ZnO. Besides, the piezoelectric effect is expected to be largely enhanced at the nano/atomic scale. Vertical piezoelectric coefficient (d_{33}) up to 33 pm•V^{-1} was determined for the chemical vapor deposition (CVD)—synthesized CdS ultrathin film
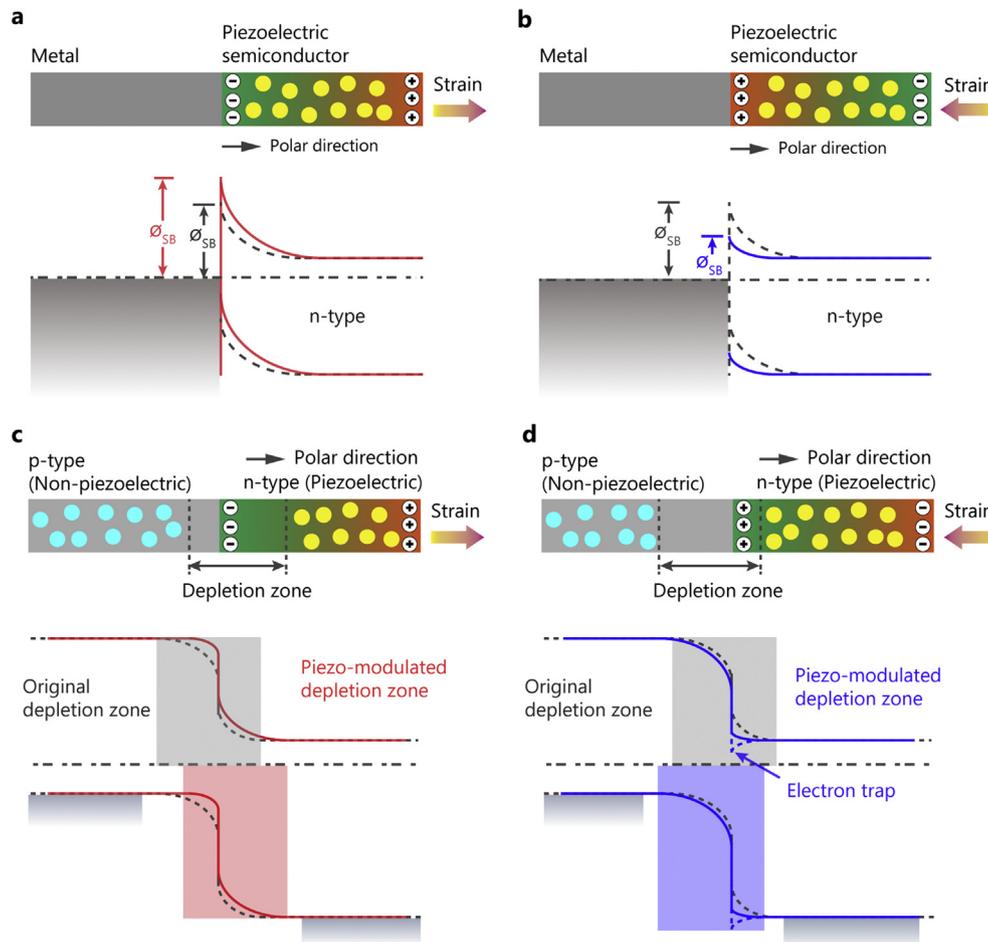
Fig. 1. Schematic for illustrating the modulation of interfacial energy-band profiles at the Schottky contact and p-n heterojunction with piezoelectric potential. The black dotted line represents original energy-band tilting under strain-free condition and zero bias, while the realigned bands affected by the positive and negative piezoelectric charges are denoted with blue and red solid line, respectively.

with thickness of 2–3 nm, which is approximately three times larger than that of the bulk CdS [56]. Wang et al. reported the synthesis of ~2 nm ZnO nanosheet, and the corresponding piezoelectric coefficient was evaluated to be ~23.7 pm•V^{-1} (Fig. 2a and b) [57]. This enhanced piezoelectricity was presumably attributed to the lower carrier concentration and the change in local polarization. Second, multiple materials which are not piezoelectric in bulk become intrinsically piezoelectric in their monolayer form because of the loss of centrosymmetry. Early studied 2D piezoelectric materials of this type is the insulating h-BN. Owing to the alternating arrangement of boron and nitride atoms in the hexagonal vertex site, the monolayer h-BN was theoretically calculated to be piezoelectric [58]. Because of the insulating property, h-BN is not suitable for piezotronics/piezophototronics, and therefore, it is not paid enough attention. Afterward, based on the density functional theory (DFT) calculation, Reed et al. predicted for the first time that many of the semiconducting monolayer hexagonal transition metal dichalcogenides (TMDCs) (MX$_2$, M = Mo, W, etc.; X = S, Se, or Te) are intrinsically piezoelectric [59]. Taking the MoS$_2$ for example, the symmetry in bulk 2H-MoS$_2$ with D_{6h} point group is reduced to D_{3h} group when thinned down to monolayer [60]. It can be seen from the top-view structure (Fig. 2c) that monolayer MoS$_2$ does not have an inversion center along the in-plane (d_{11}) direction and becomes piezoelectric. When mechanically deformed, the relative displacement between Mo^{4+} and S^{2-} ions gives rise to the emergence of piezoelectric polarization charges in the material. In 2014, Wu et al.

reported the experimental observation of piezoelectricity in atomically thin MoS$_2$ through the fabrication of flexible NGs and piezotronic device (Fig. 2d) [61]. Meanwhile, Zhu et al. quantified the piezoelectric coefficient of MoS$_2$ flakes through a method that combines laterally applied electric field and nanoindentation (Fig. 2e) [62]. Inspired by this pioneering work, the study of piezoelectricity in 2D materials starts to receive its due attention, and the exploration of novel piezoelectric monolayers springs up [63,64]. Based on the first-principles calculations, Li and Li demonstrated that several monolayer group-III monochalcogenides (MX, M = Ga or In, X = S or Se) are piezoelectric [65]. As in the case of 2H-MoS$_2$ monolayer, the MX monolayers also belong to D_{3h} point group, leading to the potential piezoelectricity in them (Fig. 2f). Fei et al. predicted the anisotropic piezoelectric effect in monolayer group-IV monochalcogenides (MX, M = Sn or Ge, X = Se or S), and piezoelectric coefficients of these monolayers are expected to be about one to two orders of magnitude larger than other frequently used piezoelectric materials (Fig. 2g) [60]. Then, another two new phases of monolayer group-IV monochalcogenides were predicted by Hu and Dong, and both of them are supposed to exhibit significant piezoelectric properties [66]. Gao and Gao calculated the piezoelectric properties of group III-V (GaP, GaAs, GaSb, etc.) buckled honeycomb monolayers and theoretically predicted that they are all good piezoelectric materials [67]. More recently, an intensive data mining for over 50,000 inorganic crystals was carried out by Cheon et al., and 325 potential
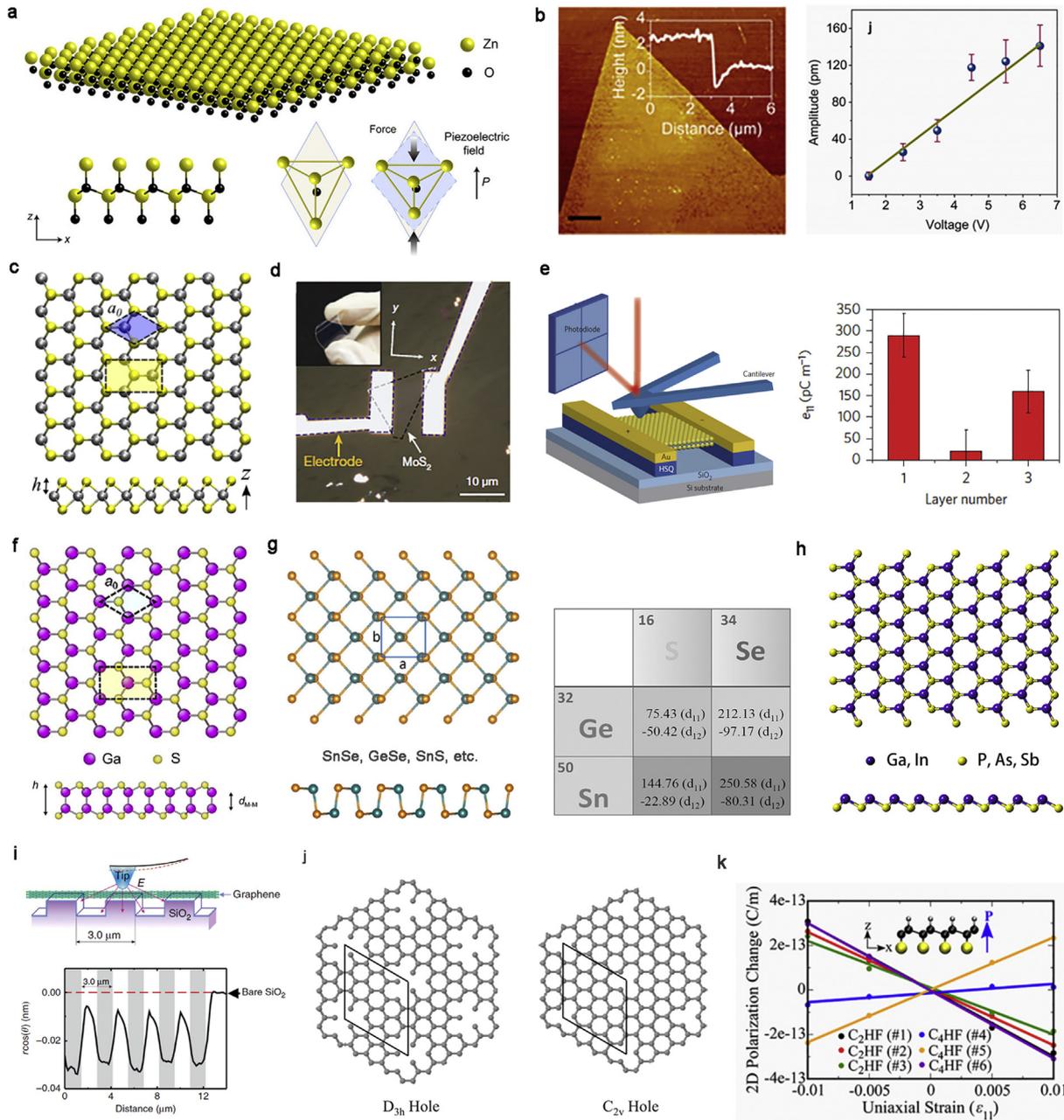
Fig. 2. (a) Schematic illustration of the ultrathin ZnO film with wurtzite structure. A piezoelectric field that points along the *c*-axis when the unit cell of ZnO nanomaterial is compressed by external force in the *z*-direction. (b) Atomic force microscopy topography of the ultrathin ZnO film and average amplitude variations vs. applied voltages [57]. (c) Monolayer top-view and side-view geometry of 2H-MoS₂ [59]. (d) A typical flexible single-layer MoS₂ nanogenerator on PET substrate with deposited electrodes at its zigzag edge [61]. (e) Schematic of the experimental setup for quantifying the piezoelectric property of freestanding MoS₂ flakes and measured piezoelectric coefficient in one-, two- and three-layer MoS₂ membranes [62]. (f) Structure model of gallium sulfide monolayer viewing from top and side [65]. (g) The typical top and side views of group-IV mono-chalcogenides orthorhombic monolayer and calculated piezoelectric coefficient [60]. (h) Top and side view of the typical 2D group III-V buckled honeycomb monolayer. (i) Schematic of the PFM measurements on single-layer graphene adsorbed on the TGZ4 grating substrate and cross-sectional of the piezoresponse along the line on graphene across the grating substrate [69]. (j) Graphical representation of the structure of two defects, D_{3h} and C_{2v} point symmetry, of the graphene that break its inversion symmetry and lead to finite in-plane piezoelectricity [71]. (k) The relationship between uniaxial strain ε_{11} and polarization charge in graphene sheet when adsorbing different configuration of C₂HF and C₄HF [72]. Reproduced with permission from: a, b, c, j, k, American Chemical Society; d, e, f, i, Springer Nature; g, AIP Publishing LLC. PET, polyethylene terephthalate; PFM, piezoresponse force microscopy.

2D piezoelectric monolayers were found [68]. The third origin of piezoelectricity in 2D materials is from the artificial surface or structure modification. A typical piezoelectric material of this type is the graphene. It is well known that graphene is not intrinsically piezoelectric because of its inversion symmetry element. However, through proper artificial manipulation of structure, a non-centrosymmetric characteristic can be introduced, leading to

possible piezoelectricity in it. Owing to the chemical interaction of carbon atoms with oxygen atoms of the underlying SiO₂ substrate, its symmetry crystal structure is broken, resulting in out-of-plane piezoelectricity in graphene (Fig. 2i) [69]. Moreover, through introducing proper structural defects (Fig. 2j) or selective adsorption of chemical molecules (Fig. 2k), finite piezoelectricity in graphene can also be achieved [70—73]. The demonstration of strong

piezoelectric effect in the fundamental limit of thickness makes 2D materials a unique platform for exploring the coupling effect between piezoelectricity and other extraordinary phenomena at the atomic scale. Meanwhile, the predicted numerous piezoelectric 2D materials provide broad selection for the fabrication of novel piezotronic and piezophototronic devices.

4. Theoretical studies of piezotronic and piezophototronic effects in 2D materials

In parallel with the exploration of novel piezoelectric 2D materials, the research on numerical simulations of piezotronic and piezophototronic effect in 2D materials has also emerged. Lopez-Suarez et al. studied the dynamics of piezoelectric h-BN monolayer by performing *ab-initio* calculations and explored their potential use in non-linear vibration energy harvesting devices [74]. In particular, a 20 nm × 1 nm h-BN monolayer under 0.3% compressive strain was predicted to harvest an electrical power of up to 0.18 pW from a 5 pN noisy vibration. Layer-dependent NG output in MoS$_2$ flakes was theoretically examined by Zhou et al. [75]. Fig. 3a shows schematic illustration of the MoS$_2$ NG and

corresponding equivalent circuit. Owing to the antiparallel stacking sequence in bulk MoS$_2$, the piezoelectric axis of each monolayer MoS$_2$ is opposed to its adjacent one [76]. Consequently, MoS$_2$ flakes with an even number of atomic layers do not exhibit piezoelectric output, while for MoS$_2$ flakes with an odd number of layers, the piezoelectric output voltage and surface piezocharges decrease with the increase of layer number, as shown in Fig. 3b. More importantly, the single-layer MoS$_2$ NG was predicted to be capable of providing satisfactory output under 1 GHZ because of its smaller capacitance, which is considerably higher than the frequency limit of ZnO nanowire−based NGs (Fig. 3c). This result suggests the promising application of MoS$_2$ NGs in high-frequency self-powered systems. In addition, Yu et al. theoretically proposed a design of new mechanoelectric NGs based on the TMDCs p-n junctions and investigated the size and doping effect [77]. For MoS$_2$ p-n homojunction with doping impurity density of 10^{13} cm^{-2} on both sides, a maximum output voltage of 0.31 V was achieved under 8% strain, indicating significantly enhanced performance over the undoped MoS$_2$ sheet (Fig. 3d). However, for WSe$_2$-MoS$_2$ heterojunction, the corresponding output voltage is only 0.185 V under 8% strain (Fig. 3e). It suggests that MoS$_2$ homojunction-based NG devices
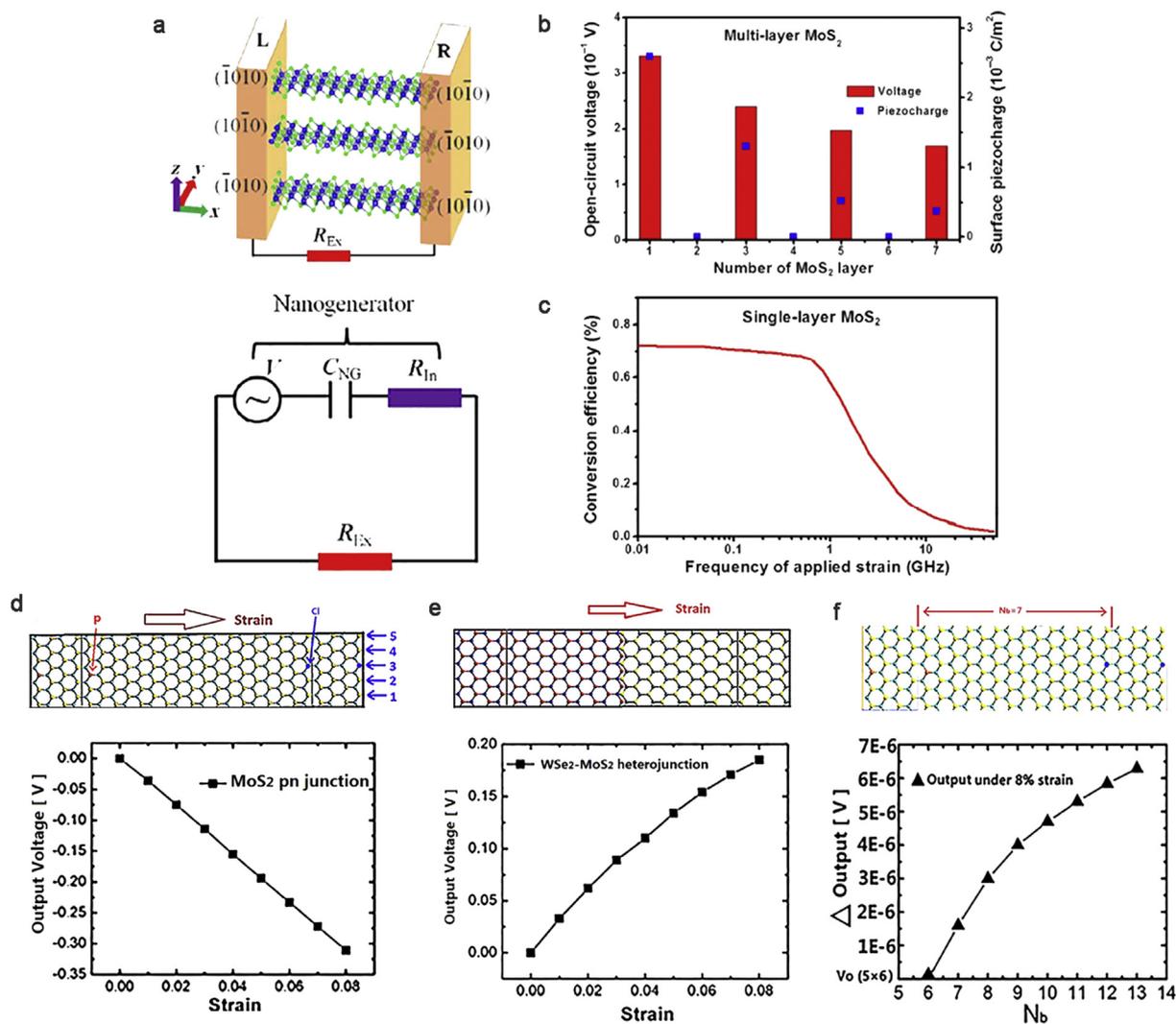
Fig. 3. (a) Schematic illustration of a three-layer MoS$_2$ NG and corresponding equivalent circuit. (b) Layer-number−dependent MoS$_2$ NG output voltage and surface piezocharges under 0.5% tensile strain. (c) Energy conversion efficiency of monolayer MoS$_2$ NG under different frequency of applied strain [75]. (d) Configuration of MoS$_2$ p-n homojunction and its output voltage as a function of strain. (e) Configuration of NG based on WSe$_2$-MoS$_2$ heterojunction and its evolution of output voltage with strain. (f) Comparison of the output voltage for MoS$_2$ nanoribbon with different length [77]. Reproduced with permission from: (a−c) and (d−f), Springer Nature. NG, nanogenerator.

possess better output performance than the TMDCs-based heterojunctions. Moreover, the output voltage of MoS$_2$ nanoribbon slightly increases by the order of magnitude of 10^{-6} V with increasing length, which indicates that the structure length has negligible effect on the NG output voltage, as shown in Fig. 3f. These results not only deepen our knowledge of piezoelectricity at the nanometer or atomic scale but also provide theoretical basis for the construction of high-efficiency and ultrathin NGs with the novel piezoelectric 2D nanomaterials.

Although the monolayer MoS$_2$ is intrinsically piezoelectric, a free-standing MoS$_2$ flat sheet was considered to be enclosed by edge-localized metallic states, which may screen the piezoelectricity and prevent the piezoelectric output [78]. Based on the DFT simulation, Liu et al. theoretically reveal the important role of metal-MoS$_2$ interface in preserving the piezoelectric effect in MoS$_2$ transistors [79]. When the free-standing MoS$_2$ contacts with a metal electrode, the bonding between metal and the edge atoms in MoS$_2$ can effectively eliminate these metallic states, which suppresses the screening effect. As shown in Fig. 4b and c, for transistors with Pd-MoS$_2$ interface contact, obvious piezopolarization

charges can be induced by applied strain and the SBH is effectively modulated. In addition, the modulation impact for different interface geometries are similar, indicating that the piezoelectric and piezotronic effects are both intrinsic properties of MoS$_2$ single layer. This result explains why the piezoelectricity in MoS$_2$ can be theoretically observed even the existence of metallic edge states and verifies the feasibility of piezotronic-modulation in novel 2D materials. Moreover, as the classical piezotronic theory faces the difficulty in explaining the mechanism of piezotronic effect for top- and enclosed-contacted MoS$_2$ transistors, Liu et al. further theoretically demonstrated that the strain-induced piezoelectric charges exist at MoS$_2$/metal-MoS$_2$ interface, which is on the electronic transport pathway rather than at the edge of MoS$_2$ flake, as shown in Fig. 4d [80]. Therefore, the charge transport characteristics in MoS$_2$ can be effectively controlled by the applied strain (Fig. 4e). This study deepens our understanding of piezotronic theory in the novel 2D materials and can serve as an important guidance for future piezotronics design. Besides the piezoelectricity, many semiconducting monolayers have also been demonstrated to possess remarkable optical properties such as direct
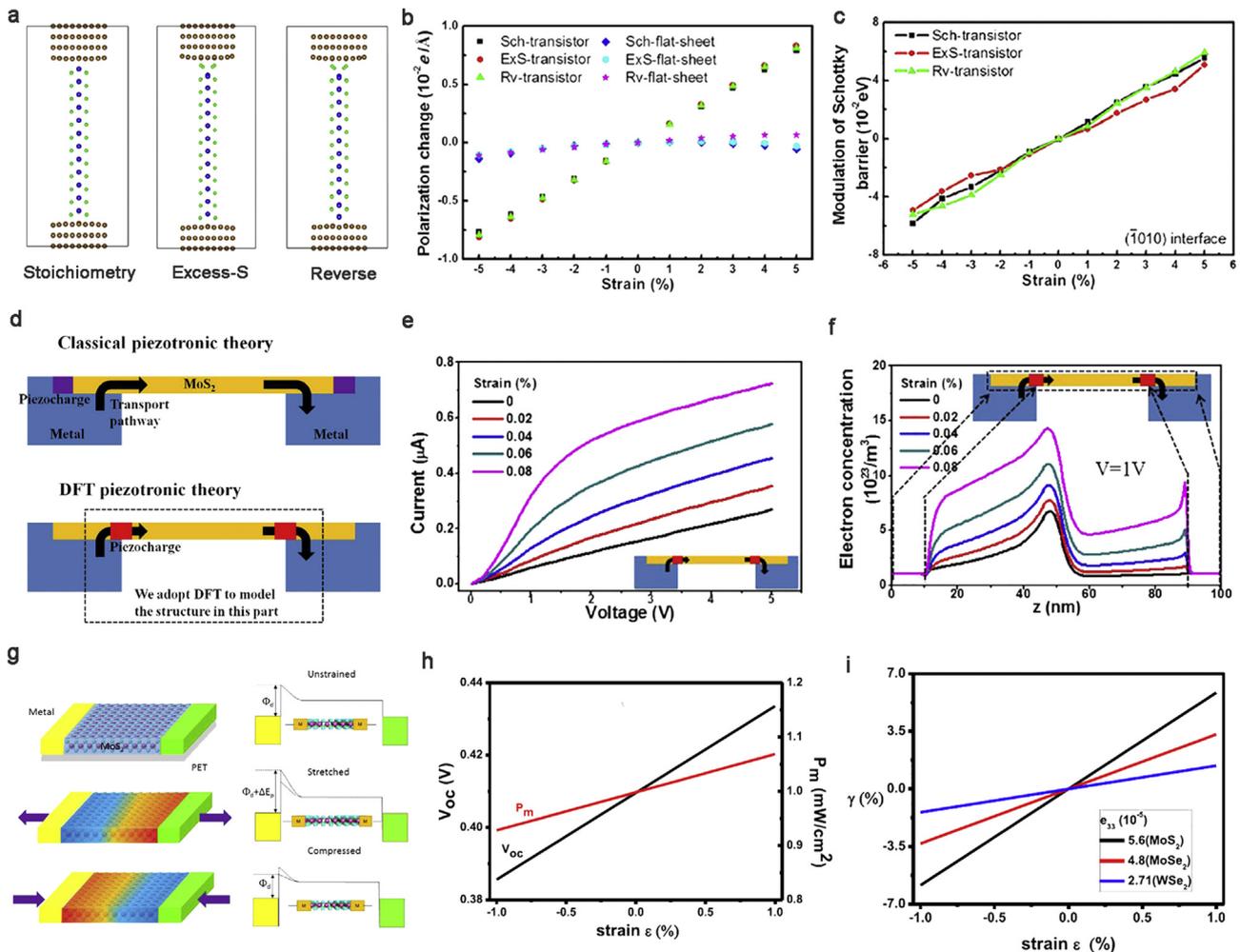
Fig. 4. (a) Three MoS$_2$ transistors with different Pd-MoS$_2$ interface contact geometries. (b) Polarizations of the transistors in (a) and free-standing MoS$_2$ sheet under strain. (c) Modulation of the Schottky barrier height of transistors with applied strain [79]. (d) Schematic illustration of the difference between the classical and DFT piezotronic theory on the piezocharges distribution in enclosed-contacted MoS$_2$ transistor. (e) The *I-V* curves of enclosed-contacted transistor under the external applied tensile strains with the piezocharges at the MoS$_2$/Pd-MoS$_2$ interface. (f) The electron concentrations in the MoS$_2$ flake along the transport direction at 1V bias [80]. (g) Schematic of the energy-band diagram in MoS$_2$ monolayer single Schottky solar cell and the band realignment under tensile/compressive strains. (h) Open-circuit voltage and maximum output power under various applied strains. (i) The comparison of piezophototronic modulation impact on MoS$_2$-, MoSe$_2$-, and WSe$_2$-based solar cells [81]. Reproduced with permission from (a–c) and (d–f), AIP Publishing LLC; (g–i), Elsevier Ltd. DFT, density functional theory.

bandgap and strong absorption of visible light, making them promising candidate for novel 2D piezophototronics. Zheng et al. theoretically simulated the piezophototronic effect in MoS$_2$ monolayer-based single Schottky solar cell, as shown in Fig. 4g [81]. The strain-induced piezopolarization charges at the interface can effectively tune the SBH and hence the performance of solar cells. The calculated open-circuit voltage was increased by 5.8% when applying a 1% strain (Fig. 4h). Moreover, it demonstrated that the modulation impact of piezophototronic effect on MoS$_2$ solar cell is higher than that on MoSe$_2$ and WSe$_2$ solar cells, as presented in Fig. 4i. This may be because the MoS$_2$ monolayer possesses the highest piezoelectric coefficient among them.

5. Piezotronic and piezophototronic applications using 2D materials

Although various monolayer structures are predicted to be intrinsically piezoelectric, only a very limited number of them have been experimentally confirmed. Until now, the monolayer MoS$_2$ remains the most studied 2D piezoelectric material because of its mature synthesizing technique and good stability under ambient condition [82]. In addition, the measured piezoelectric coefficient e_{11} of MoS$_2$ is comparable to the bulk values of standard piezoelectric crystals such as ZnO or AlN, making it suitable for piezotronics and piezophototronics fabrication [62]. In this section, we will briefly summarize the representative applications that rely on the piezoelectricity of 2D materials, hoping to provide reference for other potential 2D monolayers and inspire novel device design for the future piezotronics/piezophototronics.

5.1. NGs for energy harvesting

The piezoelectric NGs were first proposed by Wang and Song in 2006, which utilizes the piezoelectric effect of nanowires for converting tiny mechanical energy into electricity [5]. In essence, the NGs are applications of Maxwell's displacement current in energy and hold great promise for self-powered systems [9,83]. Wu et al. pioneered the work in constructing energy harvester with the piezoelectric 2D MoS$_2$ flakes [61]. The NG was fabricated by transferring mechanically exfoliated MoS$_2$ onto flexible polyethylene terephthalate (PET) substrate and deposition of Pd electrodes at the zigzag edge of MoS$_2$ to form Schottky contacts (Fig. 5a). Periodic stretching and releasing of substrate generates stable and reproducible alternating piezoelectric outputs in external circuit, as displayed in Fig. 5b. Meanwhile, layer-number dependence of piezoelectric output was also demonstrated in the MoS$_2$ NGs (Fig. 5c), which is consistent with the simulation results and measured variation trend of piezoelectric coefficient in MoS$_2$ [59,62]. For monolayer MoS$_2$ based NG, the maximum instantaneous output power at 0.53% strain is about 55.3 fW and the conversion efficiency was estimated as ~5.08%. Meanwhile, the performance of NG can be further enhanced through array integration, as shown in Fig. 5d–f.

Besides the layer-dependent piezoelectric output in MoS$_2$ NG, Kim et al. demonstrated the direction-dependent piezoelectric effect in CVD-grown triangular-shaped monolayer MoS$_2$ [84]. The measured d_{11} of MoS$_2$ in the armchair direction is about 3.78 pm V^{-1}, while the piezoelectric coefficient in the zigzag direction is only 1.38 pm V^{-1} (Fig. 6b and e). Consequently, under the same applied strain of 0.48%, the output voltage of NG with armchair direction of MoS$_2$ reached up to 20 mV. On the other hand, the generated voltage from NG with zigzag direction was less than 10 mV (Fig. 6c and f). In addition, previous research on piezoelectric ZnO nanowire NGs has demonstrated that the piezoelectric property in semiconductor is closely related with the carrier

concentration [85]. The CVD synthesized 2D materials have been demonstrated to be host to a wide range of defect types. Based on this principle, Han et al. further proposed a sulfur (S) vacancy passivation method to reduce the screening of piezopolarization charges by free carriers in MoS$_2$ [86]. After defect passivation, the carrier density in MoS$_2$ decreased from 2.19×10^{12} cm^{-2} to 6.11×10^{11} cm^{-2}. Meanwhile, the obtained piezoelectric coefficient increased from 3.06 pm•V^{-1} to 3.73 pm•V^{-1}. The NGs were fabricated to further investigate the piezoelectric property change of defect-passivated MoS$_2$ monolayer. In the case of output voltage, the S-treated devices show more than 2 times higher than that of the pristine MoS$_2$ under the same test condition. It should be mentioned that all the above mentioned NGs were fabricated by employing monolayer TMDC because these materials are predicted to have a greatly reduced or absent piezoelectricity in their multilayer form. However, Lee et al. demonstrated the reliable piezoelectric property in WSe$_2$ bilayers fabricated *via* turbostratic stacking [87]. Previous report shows that the CVD-grown WSe$_2$ bilayer (b-WSe$_2$) normally has AA′ stacking mode and lose its piezoelectricity because of the centrosymmetric structure [88]. But when artificially transferring one WSe$_2$ monolayer (m-WSe$_2$) onto another, the resulting tb-WSe$_2$ allows another four stacking modes including AA, AB, AB′ and A'B [89,90]. Among them, the AA and AB stacked b-WSe$_2$ retain a large piezoelectric coefficient that is comparable to that of m-WSe$_2$. As the transfer method alleviates restriction of geometric relationship between the two separate WSe$_2$ layers, various stacking structures are available, leading to the possible piezoelectricity in the artificial tb-WSe$_2$. Therefore, piezoresponse can be detected in these fabricated tb-WSe$_2$ and the measured d_{11} are in the range of 0–1.5 pm V^{-1}. Consequently, a part of the artificially constructed tb-WSe$_2$ can be employed to fabricate piezoelectric NGs. Moreover, as the bilayer TMDC materials have outstanding mechanical properties compared with the monolayer TMDC. The artificial tb-WSe$_2$–based piezoelectric NGs are demonstrated to show better mechanical durability. This work provides a novel approach to artificial manipulation of piezoelectricity in multilayer TMDCs and further increases the materials selectivity for NGs and piezotronics.

5.2. Piezotronic effect enhanced nanosensors

As mentioned in section 2, the piezotronic effect tunes carrier transport process through modulating interfacial barrier height, thus device current changes exponentially with the applied strain. Consequently, compared with the piezoresistive effect, which means a change in bulk electrical resistivity and typically follows a linear relationship with strain, the piezotronic sensors offer a much-enhanced sensitivity [38,91]. Wu et al. demonstrated the piezotronic effect in monolayer MoS$_2$ for the first time [61]. The fabricated metal-semiconductor-metal (MSM) structure consisted of two back-to-back Schottky barriers. For single-layer MoS$_2$ device, it can be seen from Fig. 7a that under positive drain bias, the current-voltage curve shifted leftwards under tensile strain and rightwards with compressive strain, while the opposite trend was observed under negative drain bias. This asymmetric modulation is a typical characteristic of the piezotronic effect, which originates from the asymmetric modulation of SBH with strain-induced piezopolarization charges at the zigzag edge of MoS$_2$ (Fig. 7c). However, in bilayer MoS$_2$ and bulk devices, the materials lose their piezoelectricity, therefore the strain-modulation of current displays the same trend under both the positive and negative drain bias (Fig. 7b). The highest gauge factor (the ration between current change and strain amplitude) of the monolayer MoS$_2$ piezotronic device for strain sensing is ~760, which far exceeds the value of piezoresistive MoS$_2$ and graphene-based strain sensors [92,93]. Qi
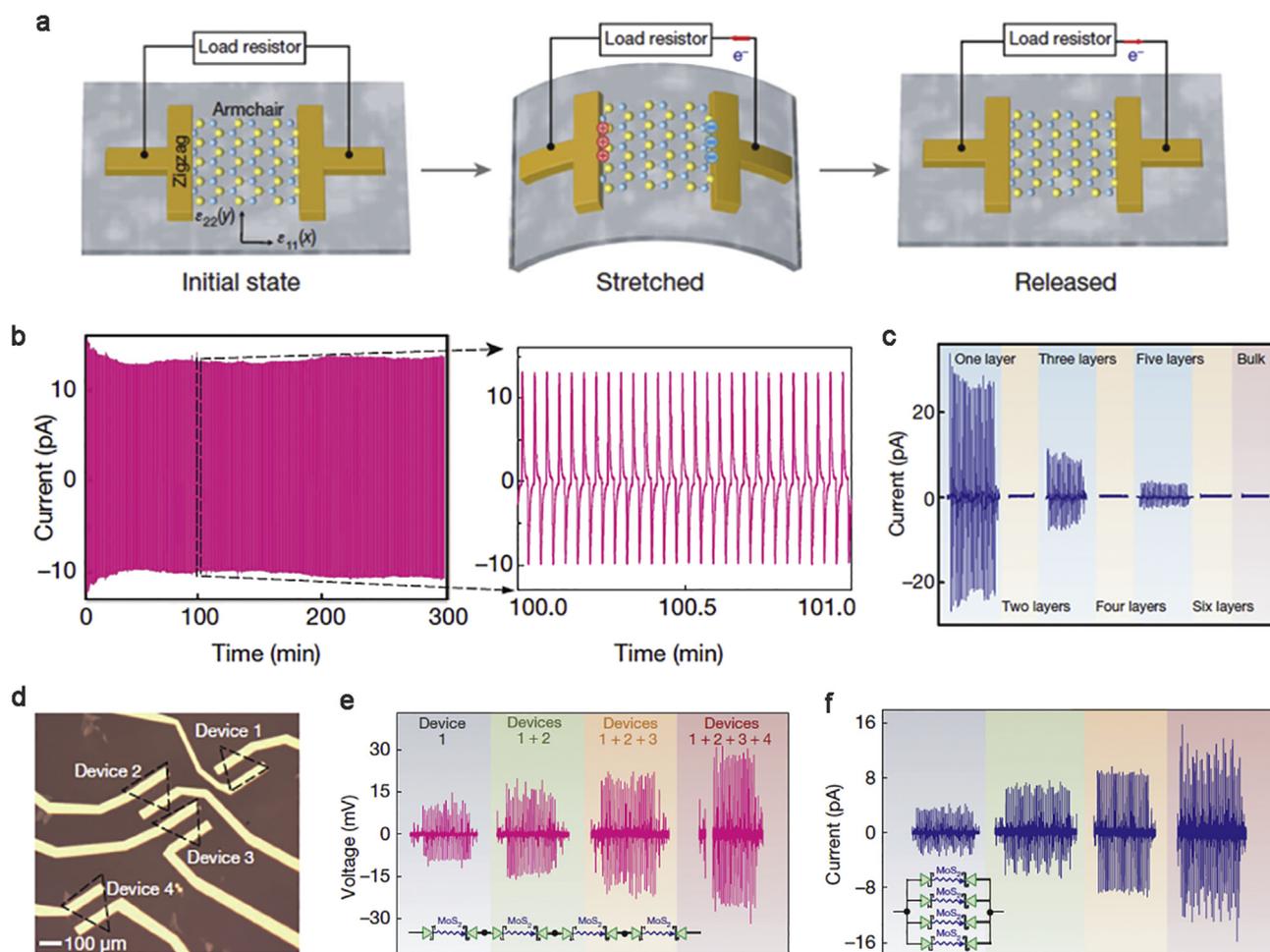
Fig. 5. (a) Operation scheme of the single-layer MoS$_2$-based piezoelectric NG. When the device is stretched, piezoelectric polarization charges with opposite polarity are induced at the zigzag edges of MoS$_2$ flake. (b) Cyclic test showing the stability of single-layer MoS$_2$ NG output. (c) Evolution of the piezoelectric outputs with increasing number of atomic layers in MoS$_2$. (d) Optical image of NG arrays consisting of four CVD single-layer MoS$_2$. (e) Constructive voltage output by serial connection of the individual MoS$_2$ flakes in the circuit. (f) Constructive current outputs by parallel connection of the MoS$_2$ flakes [61]. Reproduced with permission from Springer Nature. NG, nanogenerator; CVD, chemical vapor deposition.

et al. investigated the piezotronic effect in CVD grown triangular monolayer MoS$_2$ with the help of atomic force microscope (AFM), as shown in Fig. 7d [94]. Different from the bending of flexible polymer substrate, the AFM tip was adopted to introduce strain in their fabricated devices. The amplitude of strain was controlled through manipulating applied loading force and the strain direction can be varied with the loading locations (Fig. 7e). The result indicates effective mechanical tuning of electronic transport properties in the devices, which can be attributed to the piezotronic effect. The highest gauge factor in the monolayer MoS$_2$ piezotronic devices is about 1160, which shows their great application potential in strain/stress sensors and strain-gated logic units. Time-resolved measurement of the current response over repeated compressive and tensile strain is shown in Fig. 7f and g. The rise and decay time of MoS$_2$ strain sensor were about 1.79 and 1.23 s, respectively, and the device displays excellent response repeatability and stability.

Owing to the effective modulation of interface properties, the piezotronic effect can also be employed to enhance performance of Schottky-contacted sensors. This application has been extensively demonstrated in wurtzite ZnO- and GaN-based devices [95−98]. Compared with the 1D morphology, the 2D materials possess exceedingly high surface-to-volume ratio and hence more reactive sites for redox reactions, making them promising building blocks

for highly responsive chemical sensors [99−101]. By taking advantage of the piezoelectricity in 2D TMDC, Guo et al. reported the piezotronic-enhanced flexible humidity sensing of monolayer MoS$_2$ [102]. The device was fabricated with two back-to-back Pd-MoS$_2$ Schottky junctions on flexible PET substrate (Fig. 8a). In this configuration, the transport property was limited by the reverse-biased Pd-MoS$_2$ SBH and can be effectively modulated by the piezopolarization charges. The sensing property of device under different relative humidity and applied strains is plotted in Fig. 8b. It can be seen that the response current increases with increasing tensile strain, indicating an enhanced sensitivity. Energy-band diagrams were drawn to schematically illustrate the piezotronic effect, as shown in Fig. 8c and d. When applying tensile strain, the induced positive piezopolarization charges at the zigzag edge of MoS$_2$ decreases SBH. Consequently, more electrons can transport across the junction interface, leading to increased device response current. Furthermore, experimental results also show that the modulation impact of piezotronic effect is weaker for high relative humidity. It may be because that with increasing the humidity, more water molecules are absorbed on the MoS$_2$ surface. The accumulation of free electrons at the vicinity of Schottky contact area results in partial screening of piezocharges, thus weakening the piezotronic effect [103].
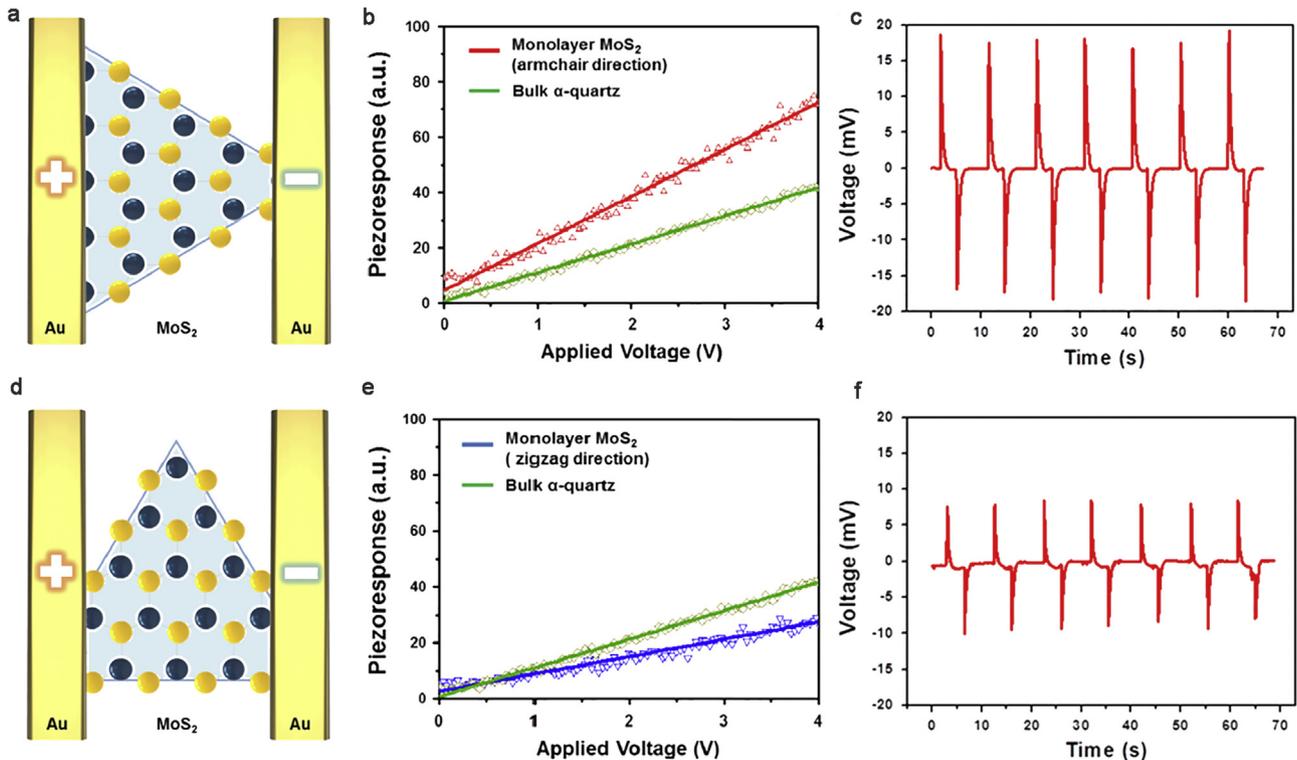
Fig. 6. Lateral electrode configuration to measure the d_{11} of triangular MoS$_2$ monolayer according to the electric field applied in the direction of (a) armchair and (d) zigzag. Corresponding piezoresponse for the MoS$_2$ in the (b) armchair and (e) zigzag direction, respectively. Voltage outputs of the NGs by applying the same strain along (c) armchair and (f) zigzag directions [84]. Reproduced with permission from Elsevier Ltd. NG, nanogenerator.

5.3. Piezophototronic effect on 2D materials—based photodetectors

Photodetectors represent semiconductor devices that can measure photon flux or optical power by converting the absorbed photon energy into electrical current [104]. They are widely used in various fields, including digital imaging, environmental monitoring, and astronomy. Generally, three processes are involved in the operation of photodetectors: (1) carrier generation by incident light, (2) carriers transport and/or multiplication if present, (3) extraction of carriers as output current. For Schottky or p-n junction—based photodetectors, each process is closely related with the interface property and eventually determines the ultimate device performance. Thus, the precise tunability over interface properties is critical to the operation of photodetectors. Recently, particular attention has been paid to the 2D layered semiconductors for application in flexible photodetectors due to their unique electronic, mechanical, and optoelectronic properties [31,62,105,106]. Conventionally, the manipulation of 2D materials-based interface property is achieved by electrostatic gating on hard substrate [107,108]. However, when applying this gate-modulation method to flexible optoelectronics, extra fabrication complexity would be introduced including the deposition of high-quality dielectric layer and gate electrode. As plenty of 2D monolayers are predicted to be intrinsically piezoelectric, the piezophototronic effect can be employed as an alternative approach to realize such interface regulation. Wu et al. reported the first experimental demonstration of piezophototronic effect in single atomic layer MoS$_2$-based flexible photodetector [109]. The device has similar MSM structure with the above mentioned piezotronic strain and humidity sensors, as shown in Fig. 9a. By modulating the separation and transport of photogenerated carriers at the MoS$_2$-metal interface, a maximum photoresponsivity

of 2.3×10^4 A W^{-1} was achieved under 3.4 µW cm^{-2} 633 nm laser illumination, which presents a 26-fold improvement over the reported highest result for monolayer MoS$_2$ phototransistors [110]. Soon afterward, the piezophototronic effect was further demonstrated in other types of MoS$_2$-based p-n junction photodetectors. A flexible mixed-dimensional heterojunction photodetector was fabricated with CVD-grown n-MoS$_2$ and *p*-CuO film on PET substrate [111]. Under a tensile strain of 0.65%, the photoresponse current for 532 nm laser can be enhanced 27 times compared with the strain-free condition and the detection sensitivity reaches up to 3.27×10^8 Jones, as shown in Fig. 9e and f. Furthermore, because of the absence of band discontinuity and lower resistance conductive path than heterojunction, the 2D homojunctions are considered to be more preferable for photodetectors [112,113]. Zhang et al. fabricated a monolayer MoS$_2$ lateral p-n junction through selective AuCl$_3$ doping for flexible photodiode, and the performance enhancement was also achieved with piezophototronic effect (Fig. 9g) [114]. When applying a 0.51% static tensile strain, the photoresponsivity and detectivity of device reach up to 1161 A W^{-1} and 1.72×10^{12} Jones, indicating 619% and 319% enhancement compared with the strain-free state (Fig. 9h). This performance improvement was attributed to the broadening of depletion zone in the p-n junction by piezophototronic effect, which benefits the separation and transport process of photogenerated carriers (Fig. 9i). Lin et al. demonstrated the piezophototronic-enhanced flexible n-MoS$_2$/p-WSe$_2$ all-2D vdWs photodiode (Fig. 9j) [115]. Under the 1.52 mW cm^{-2} 532 nm illumination and zero bias, an optimized photoresponsivity of ~3.4 mA W^{-1} was achieved when introducing a −0.62% compressive strain. In this case, the compressive strain-induced positive piezopolarization charges in MoS$_2$ function as an applied reverse bias, providing extra driving force for the rapid
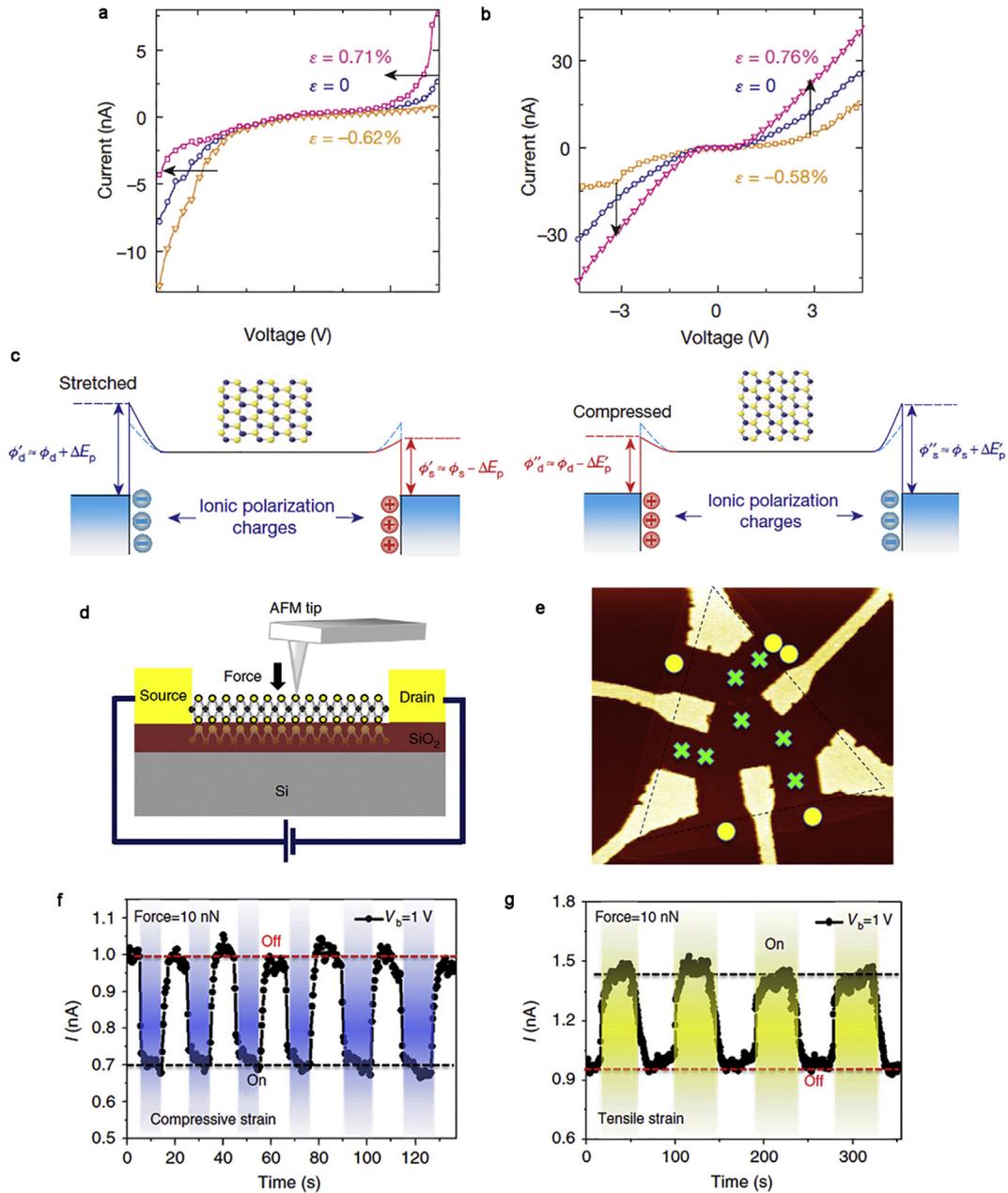
Fig. 7. Electrical characterizations of the (a) monolayer and (b) bilayer MoS$_2$ devices under different strains, which show typical asymmetric and symmetric modulation behavior, respectively. (c) Energy-band diagrams explaining the piezotronic effect in the single-layer MoS$_2$ device [61]. (d) Schematic illustration of a MoS$_2$ piezotronic device under mechanical load by AFM tip. (e) The relation between loading position and strain polarity. Loading force on the yellow circle positions generates tensile strains in MoS$_2$, while applying force on green cross positions with AFM tip generates compressive strains. Current response of the MoS$_2$ piezotronic strain sensor under repeated (f) compressive and (g) tensile strain at a fixed drain bias of 1 V [94]. AFM, atomic force microscope. Reproduced with permission from Springer Nature.

separation of photogenerated carriers. As a consequence, the injection of photoexcited electrons in WSe$_2$ into MoS$_2$ was promoted more effectively, leading to improved photocurrent (Fig. 9l). However, with the further increase of compressive strain, a decrease of photocurrent was observed. This could be because of the formation of electron traps in MoS$_2$ under the influence of high-density piezocharges, which jeopardizes the extraction process of carriers and decreases the response current. The piezophototronic effect offers 2D optoelectronics another way to interact with external mechanical stimuli, which may inspire new structure design for novel ultrathin devices and broaden their applications in wearable devices and human-machine interfacing.

6. Prospects of 2D materials for piezotronics and piezophototronics

Inspired by the pioneering work based on MoS$_2$, the research of novel piezoelectric 2D materials and devices is expected to intensify in the coming years [116–118]. At the time of writing this article, the existence of more than dozens of piezoelectric 2D crystals has been theoretically predicted, but most of them need to be further experimentally confirmed. In this regard, some rule of thumb may be helpful to screen the potential 2D candidates for further novel piezotronics and piezophototronics. First, the piezoelectric coefficient should be considered as a priority. The high
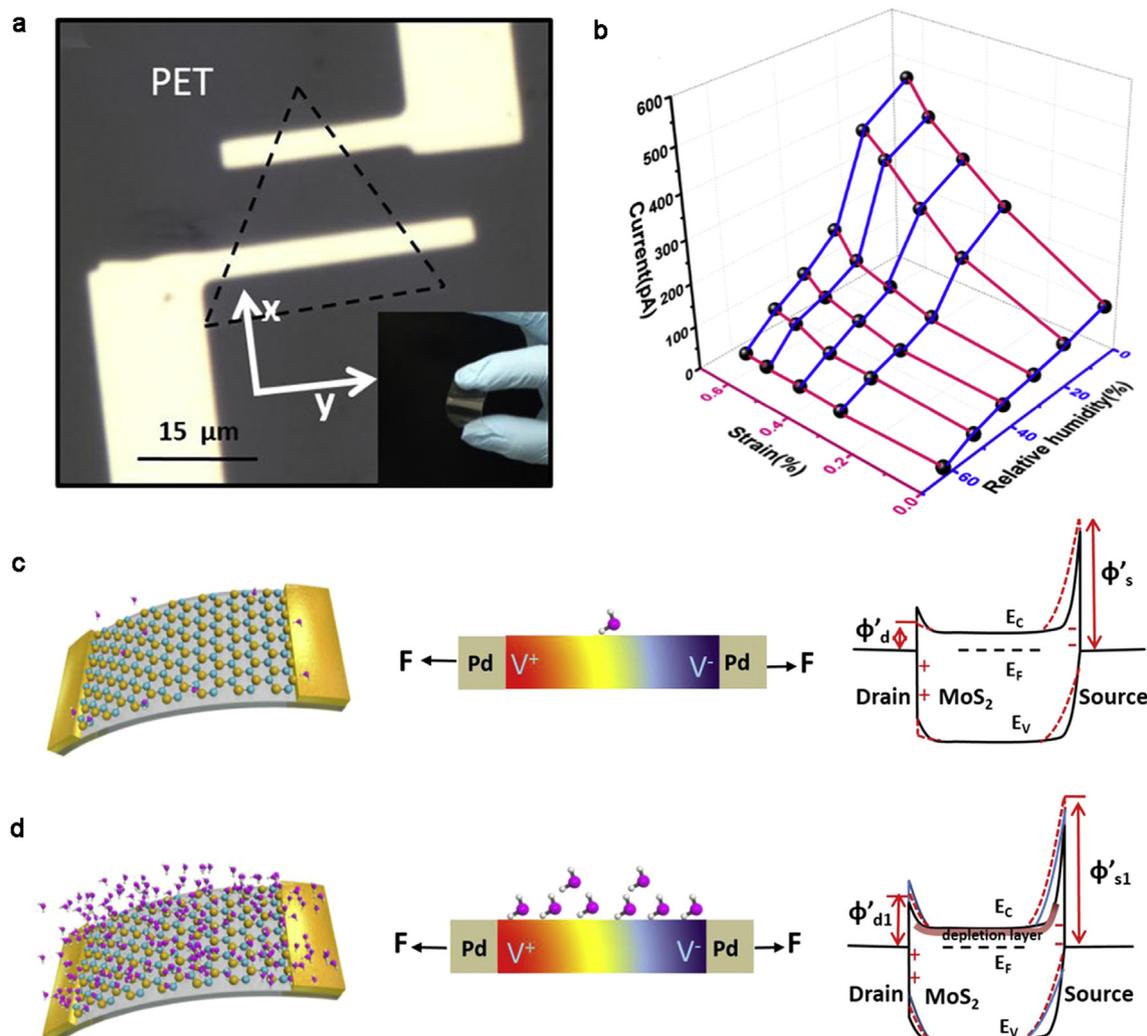
Fig. 8. (a) Optical image of the flexible monolayer MoS$_2$ humidity sensor on PET substrate. (b) Three-dimensional plot depicting the current response of humidity sensor under different strains and relative humidity at a bias of 10 V. Schematic energy-band diagrams illustrating the piezotronic effect on sensing performance under (c) low and (d) high humidity conditions, respectively [102]. Reproduced with permission from American Chemical Society. PET, polyethylene terephthalate.

piezoelectric coefficient can guarantee the dominant role of piezotronic/piezophototronic effect in device performance modulation, rather than the piezoresistivity or metal-semiconductor contact change. Second, the materials should have favorable semiconducting and optoelectric properties. It is the basis for the fabrication of high-performance piezotronic/piezophototronic devices. Third, it is preferable that the materials possess good thermal/chemical stability and survive under ambient condition. However, this is not a necessary qualification from the viewpoint of scientific research because the manipulation of novel 2D materials at low temperature or in an inert atmosphere is no more a limitation. Fourth, it can be best that the preparation method of materials is controllable and reproducible, so the variations in materials quality and piezotronics/piezophototronics performance can be reduced. Based on the above-mentioned criteria, we propose several kinds of 2D materials that are worthy of future investigation for novel piezotronics/piezophototronics:

(1) Transition metal dichalcogenides: it is undeniable that TMDCs have the most mature processing technique among the novel 2D materials beyond graphene. Although the MoS$_2$-based piezotronics/piezophototronics have been widely reported, the research toward materials of this type is far from being exhausted. For instance, epitaxial growth of monolayer TMDCs-based lateral heterojunctions has been demonstrated with their photoelectric property being thoroughly probed [119–121]. However, the corresponding piezoelectric properties of these alloyed structures still remain unknown. In addition, the dangling band-free surfaces of TMDCs allow the arbitrary stacking of distinct materials in a chosen sequence as in building with Lego [122]. In this regard, is there any possibility that we can achieve the arbitrary manipulation of piezoelectric property at the atomic scale by using the similar method? Moreover, besides the all-2D vdWs contact, the mixed-dimensional vdWs heterostructures by hybridizing 2D TMDCs with other materials of different dimensionality have also attracted interests of researchers [123]. This will foster a whole new area of applications for the piezotronic/piezophototronic effect.

(2) Metal oxides: the research of metal oxides has always been one of the important research branches in material science [124]. Recent theoretical simulation indicates that monolayer group-II oxides are piezoelectric with relatively high piezoelectric coefficient. The combination of piezoelectricity with
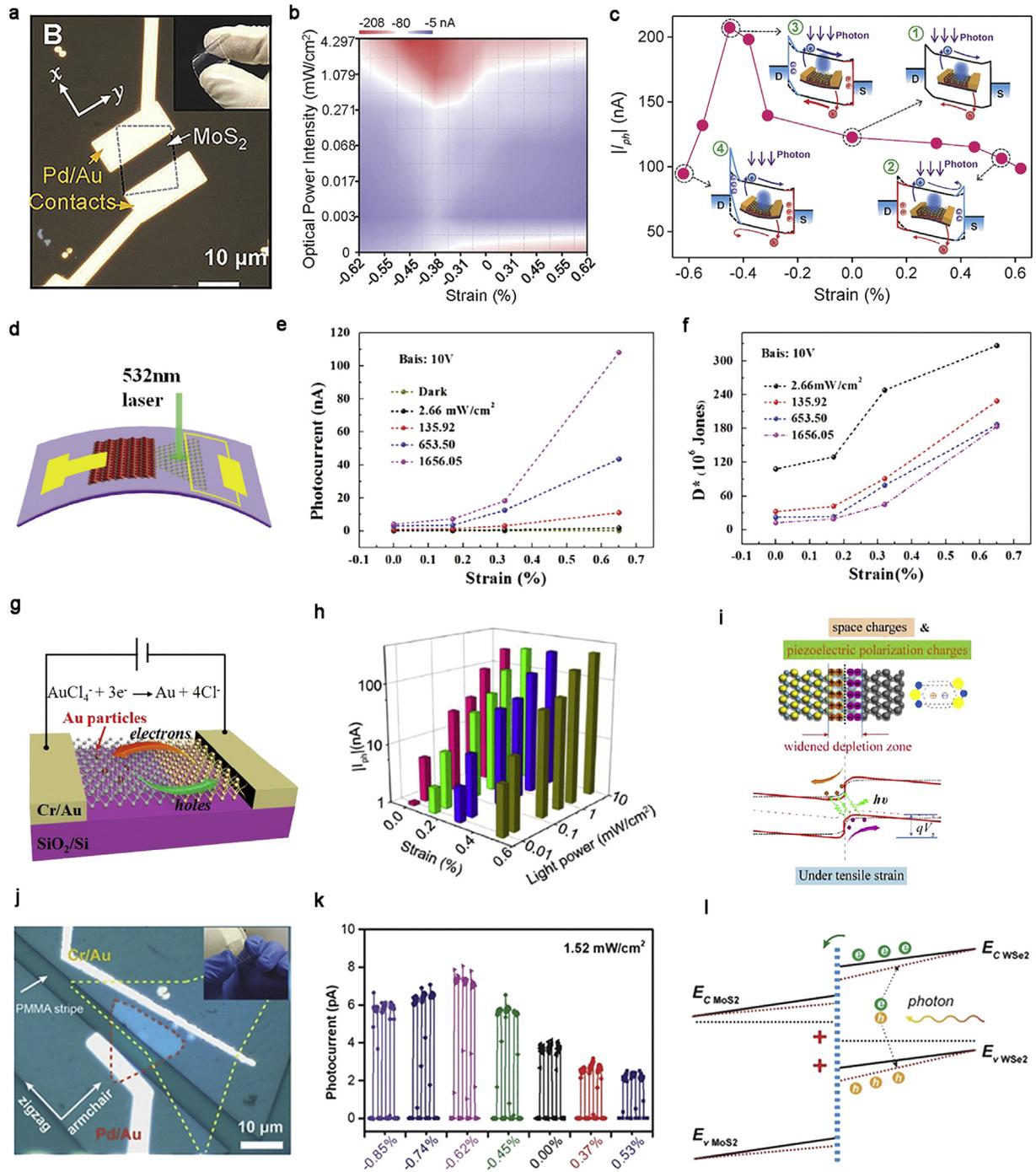
Fig. 9. (a) A flexible monolayer MoS₂ piezophototronic device with MSM structure. (b) Piezophototronic mapping for photocurrent in the device under different illumination intensities and mechanical strains. (c) Working mechanism of the piezophototronic modulation process in monolayer MoS₂ photodetector [109]. (d) Schematic illustration of the flexible photodetector based on p-CuO/n-MoS₂ heterojunction. The strain dependence of (e) photocurrent and (f) detectivity under different illumination power [111]. (g) Schematic of monolayer MoS₂ lateral p-n homojunction photodiode. (h) The variation of device photocurrent under different optical power and applied strains. (i) Working mechanism of the piezophototronic-modulated MoS₂ p-n homojunction photodetector [114]. (j) Optical image of the flexible MoS₂/WSe₂ all-2D van der Waals photodiode. (k) Strain dependence of photocurrent in the device under the illumination of 1.52 mW cm⁻² light. (l) Energy-band profile change at the junction interface when positive piezocharges are induced in MoS₂ under compressive strain [115]. MSM, metal-semiconductor-metal. Reproduced with permission from: (a—c) and (j—l), John Wiley & Sons, Inc.; (d—f), Royal Society of Chemistry; (g—i), IOP Publishing Ltd.

conventional oxide devices may bring novel breakthroughs in device design concepts and applications.

(3) Layered perovskite materials: the perovskites have been attracting significant attention in recent years for their excellent intrinsic optoelectronic properties, such as direct bandgap, large absorption coefficient, and high carrier mobility [125,126]. From the viewpoint of crystallography, the perovskites are intrinsically piezoelectric. It can be sure that the piezophototronic effect holds great potential for applications in perovskite-based optoelectronics such as solar cells,

photodetectors, and light emitters. However, the 2D perovskites–based piezophototronics are scarcely reported until now.

(4) Organic 2D crystals: so far, almost all the reported piezotronics/piezophototronics are fabricated with inorganic materials. Nevertheless, the recent rise of organic 2D crystals may offer a possibility for extending this novel device concept to a new area [127,128]. At present, the piezoelectric property of organic 2D semiconductors is still poorly understood. However, considering the extensive applicative prospect of organic 2D materials in flexible/stretchable electronics and optoelectronics, this topic is well worth our exploration. In short, with the synthetic and assembly advances of piezoelectric 2D materials, much work remains to be done to make the full use of their potential in novel piezotronics/piezophototronics.

7. Summary and outlook

After more than 13 years of worldwide intensive efforts, the research of piezotronics/piezophototronics has become a significant study area and attracted researchers from a wide range of disciplines, including condensed matter physics, materials science, electrical engineering, chemistry, and even the biology. Piezotronic and piezophototronic effects are inevitable in the third-generation semiconductors. Owing the 2D confinement and spontaneous breaking of inversion symmetry, plenty of materials are theoretically predicted to be piezoelectric in their 2D forms. The integration of piezoelectricity and other intriguing properties in 2D materials provide a new platform for the exploration of novel physics at the atomic scale as well as potential device applications. Therefore, it is believed that the 2D piezotronics/piezophototronics will be one of the important research branches in this emerging field. Although the fundamental principle of piezotronic/piezophototronic effects have been well established, our understanding on the coupling behavior between piezoelectricity and semiconductor properties still needs to be enhanced. For instance, most of the previous numerical studies on piezotronic/piezophototronic effects are based on the finite element method. Now the observation of piezoelectricity in the fundamental thickness limit allows us to investigate these effects from the first-principles calculations, which may provide a more accurate interpretation of the underlying mechanism. So far, varieties of proof-of-concept devices have been demonstrated by using piezoelectricity in the 2D materials for potential applications in energy harvesting, ultrathin actuators, adaptive electronics, and optoelectronics. There is no doubt that outstanding opportunities for innovation exist in this emerging field but with the great challenges on the road ahead.

(1) Further study on the piezoelectricity in 2D materials is required. On the one hand, more predicted piezoelectric 2D materials need to be validated with experimental methods. In addition, parameters influencing the 2D piezoelectricity should be identified so that the artificial manipulation of piezoelectric property at the atomic scale can be achieved. For example, design of specific piezoelectric structures may be realized through arbitrary stacking of vdWs monolayers or chemical functionalization of the 2D materials.

(2) From the viewpoint of scientific research, the combination of piezoelectricity with other unique properties in 2D materials looks more promising than ever before. The topological insulating phase, intrinsic ferromagnetism, and quantum spin Hall effect have been demonstrated in 2D crystals [129–132]. It is possible to use the piezotronic effect to control the quantum or spin transport process, ultimately leading to novel device applications or scientific breakthroughs in new physics. Now the coupling research among mechanical strain, piezoelectricity/ferroelectricity, and ferromagnetism in novel 2D materials has not yet been reported, but we suppose that it is much worthy of intensive study.

(3) So far, most of the reported interpretation of piezotronic/piezophototronic effects are normally based on the qualitative analysis of energy band. However, from the viewpoint of application, quantitative characterization methods are needed. It will not only help to distinguish the role of piezotronic/piezophototronic effect from other influencing factors but also provide guidelines for the engineering of piezoelectric 2D semiconductors.

(4) The growing interest in novel 2D piezotronics/piezophototronics is not only limited to new physics but also to the massive potential for applications because of their easy integration with the well-developed semiconductor process. Nevertheless, to realize practical application, the same priority should be placed on the stability and durability of devices [133]. Further studies in this direction are necessary and much work remains to be done from the following aspects, such as the controllability of materials' piezoelectric property, the reliability of metal-semiconductor contact under strain, the influence of ambient atmosphere and encapsulation technology, etc.

Overall, the emergence of piezoelectric 2D materials has expanded the piezotronics/piezophototronics research dramatically and reserved one of the leading topics in the coming years. By combing this new device concept with the rising 2D materials system, novel devices have been demonstrated with potential applications in energy harvesting, flexible/stretchable electronics, human-machine interfacing, and self-powered systems. Considering the possible breakthroughs in new physics and their massive application potential on industrial scale, more endeavor is still needed to explore the full potential of this exciting research field.

Conflict of interest

The authors declared that they have no conflicts of interest to this work.

Acknowledgments

References

[1] A.I. Kingon, S. Srinivasan, Nat. Mater. 4 (2005) 233–237.
[2] S.R. Khaled, D. Sameoto, S. Evoy, Smart Mater. Struct. 23 (2014), 033001.
[3] C. Ribeiro, C.M. Costa, D.M. Correia, J. Nunes-Pereira, J. Oliveira, P. Martins, R. Gonçalves, V.F. Cardoso, S. Lanceros-Méndez, Nat. Protoc. 13 (2018) 681.
[4] S. Horiuchi, Y. Tokura, Nat. Mater. 7 (2008) 357–366.
[5] Z.L. Wang, J. Song, Science 312 (2006) 242–246.
[6] S. Xu, Y. Qin, C. Xu, Y. Wei, R. Yang, Z.L. Wang, Nat. Nanotechnol. 5 (2010) 366–373.
[7] Z.L. Wang, X. Wang, J. Song, J. Liu, Y. Gao, IEEE Pervasive Comput. 7 (2008) 49–55.
[8] Y. Hu, Z.L. Wang, Nano Energy 14 (2015) 3–14.
[9] X. Wang, Nano Energy 1 (2012) 13–24.
[10] Z.L. Wang, Adv. Mater. 19 (2007) 889–892.
[11] Z.L. Wang, Nano Today 5 (2010) 540–552.
[12] Z.L. Wang, J. Phys. Chem. Lett. 1 (2010) 1388–1393.

[13] Z.L. Wang, W. Wu, Natl. Sci. Rev. 1 (2014) 62–90.
[14] W. Wu, Z.L. Wang, Nat. Rev. Mater. 1 (2016) 16031.
[15] W. Wu, X. Wen, Z.L. Wang, Science 340 (2013) 952–957.
[16] C. Pan, L. Dong, G. Zhu, S. Niu, R. Yu, Q. Yang, Y. Liu, Z.L. Wang, Nat. Photonics 7 (2013) 752–758.
[17] W. Wu, Y. Wei, Z.L. Wang, Adv. Mater. 22 (2010) 4711–4715.
[18] W. Wu, Z.L. Wang, Nano Lett. 11 (2011) 2779–2785.
[19] J. Nie, G. Hu, L. Li, Y. Zhang, Nano Energy 46 (2018) 423–427.
[20] Z.L. Wang, MRS Bull. 37 (2012) 814–827.
[21] H. Liu, Q. Hua, R. Yu, Y. Yang, T. Zhang, Y. Zhang, C. Pan, Adv. Funct. Mater. 26 (2016) 5307–5314.
[22] Q. Yang, W. Wang, S. Xu, Z.L. Wang, Nano Lett. 11 (2011) 4012–4017.
[23] Q. Yang, X. Guo, W. Wang, Y. Zhang, S. Xu, D.H. Lien, Z.L. Wang, ACS Nano 4 (2010) 6285–6291.
[24] C. Pan, S. Niu, Y. Ding, L. Dong, R. Yu, Y. Liu, G. Zhu, Z.L. Wang, Nano Lett. 12 (2012) 3302–3307.
[25] K.S. Novoselov, A.K. Geim, S.V. Morozov, D. Jiang, Y. Zhang, S.V. Dubonos, I.V. Grigorieva, A.A. Firsov, Science 306 (2004) 666–669.
[26] M. Chhowalla, H.S. Shin, G. Eda, L.-J. Li, K.P. Loh, H. Zhang, Nat. Chem. 5 (2013) 263–275.
[27] M. Xu, T. Liang, M. Shi, H. Chen, Chem. Rev. 113 (2013) 3766–3798.
[28] G.R. Bhimanapati, Z. Lin, V. Meunier, Y. Jung, J. Cha, S. Das, D. Xiao, Y. Son, M.S. Strano, V.R. Cooper, L. Liang, S.G. Louie, E. Ringe, W. Zhou, S.S. Kim, R.R. Naik, B.G. Sumpter, H. Terrones, F. Xia, Y. Wang, J. Zhu, D. Akinwande, N. Alem, J.A. Schuller, R.E. Schaak, M. Terrones, J.A. Robinson, ACS Nano 9 (2015) 11509–11539.
[29] G. Fiori, F. Bonaccorso, G. Iannaccone, T. Palacios, D. Neumaier, A. Seabaugh, S.K. Banerjee, L. Colombo, Nat. Nanotechnol. 9 (2014) 768–779.
[30] F. Xia, H. Wang, D. Xiao, M. Dubey, A. Ramasubramaniam, Nat. Photonics 8 (2014) 899–907.
[31] D. Akinwande, C.J. Brennan, J.S. Bunch, P. Egberts, J.R. Felts, H. Gao, R. Huang, J.-S. Kim, T. Li, Y. Li, K.M. Liechti, N. Lu, H.S. Park, E.J. Reed, P. Wang, B.I. Yakobson, T. Zhang, Y.-W. Zhang, Y. Zhou, Y. Zhu, Extreme Mech. Lett. 13 (2017) 42–77.
[32] Y. Liu, N.O. Weiss, X. Duan, H.-C. Cheng, Y. Huang, X. Duan, Nat. Rev. Mater. 1 (2016) 16042.
[33] K.S. Novoselov, A. Mishchenko, A. Carvalho, A.H. Castro Neto, Science 353 (2016) aac9439.
[34] W. Wu, C. Pan, Y. Zhang, X. Wen, Z.L. Wang, Nano Today 8 (2013) 619–642.
[35] C. Du, W. Hu, Z.L. Wang, Adv. Eng. Mater. 20 (2017) 1700760.
[36] J. Zhou, Y. Gu, P. Fei, W. Mai, Y. Gao, R. Yang, G. Bao, Z.L. Wang, Nano Lett. 8 (2008) 3035–3040.
[37] R. Yu, W. Wu, Y. Ding, Z.L. Wang, ACS Nano 7 (2013) 6403–6409.
[38] R. Yu, S. Niu, C. Pan, Z.L. Wang, Nano Energy 14 (2015) 312–339.
[39] Z.L. Wang, Adv. Mater. 24 (2012) 4632–4646.
[40] P. Lin, X. Yan, F. Li, J. Du, J. Meng, Y. Zhang, Adv. Mater. Interfaces 4 (2016) 1600842.
[41] P. Lin, X. Yan, Z. Zhang, Y. Shen, Y. Zhao, Z. Bai, Y. Zhang, ACS Appl. Mater. Interfaces 5 (2013) 3671–3676.
[42] P. Lin, X. Chen, X. Yan, Z. Zhang, H. Yuan, P. Li, Y. Zhao, Y. Zhang, Nano Res 7 (2014) 860–868.
[43] L. Zhu, P. Lin, B. Chen, L. Wang, L. Chen, D. Li, Z.L. Wang, Nano Res 11 (2018) 3877–3885.
[44] P. Lin, L. Zhu, D. Li, L. Xu, Z.L. Wang, Nanoscale 10 (2018) 14472–14479.
[45] C. Pan, M. Chen, R. Yu, Q. Yang, Y. Hu, Y. Zhang, Z.L. Wang, Adv. Mater. 28 (2015) 1535–1552.
[46] X. Han, W. Du, R. Yu, C. Pan, Z.L. Wang, Adv. Mater. 27 (2015) 7963–7969.
[47] P. Lin, X. Yan, Y. Liu, P. Li, S. Lu, Y. Zhang, Phys. Chem. Chem. Phys. 16 (2014) 26697–26700.
[48] Y. Zhang, Y. Liu, Z.L. Wang, Adv. Mater. 23 (2011) 3004–3013.
[49] Y. Zhang, Z.L. Wang, Adv. Mater. 24 (2012) 4712–4718.
[50] Y. Zhang, Y. Yang, Z.L. Wang, Energy Environ. Sci. 5 (2012) 6850–6856.
[51] Y. Liu, S. Niu, Q. Yang, B.D.B. Klein, Y.S. Zhou, Z.L. Wang, Adv. Mater. 26 (2014) 7209–7216.
[52] Y. Liu, Y. Zhang, Q. Yang, S. Niu, Z.L. Wang, Nano Energy 14 (2015) 257–275.
[53] Q. Yang, Y. Liu, C. Pan, J. Chen, X. Wen, Z.L. Wang, Nano Lett. 13 (2013) 607–613.
[54] Z. Jin, S.A. Meguid, Semicond. Sci. Technol. 32 (2017), 043006.
[55] R. Hinchet, U. Khan, C. Falconi, S.-W. Kim, Mater. Today 21 (2018) 611–630.
[56] X. Wang, X. He, H. Zhu, L. Sun, W. Fu, X. Wang, L.C. Hoong, H. Wang, Q. Zeng, W. Zhao, J. Wei, Z. Jin, Z. Shen, J. Liu, T. Zhang, Z. Liu, Sci. Adv. 2 (2016) e1600209.
[57] L. Wang, S. Liu, G. Gao, Y. Pang, X. Yin, X. Feng, L. Zhu, Y. Bai, L. Chen, T. Xiao, X. Wang, Y. Qin, Z.L. Wang, ACS Nano 12 (2018) 4903–4908.
[58] K.H. Michel, B. Verberck, Phys. Rev. B 80 (2009) 224301.
[59] K.-A.N. Duerloo, M.T. Ong, E.J. Reed, J. Phys. Chem. Lett. 3 (2012) 2871–2876.
[60] R. Fei, W. Li, J. Li, L. Yang, Appl. Phys. Lett. 107 (2015) 173104.
[61] W. Wu, L. Wang, Y. Li, F. Zhang, L. Lin, S. Niu, D. Chenet, X. Zhang, Y. Hao, T.F. Heinz, J. Hone, Z.L. Wang, Nature 514 (2014) 470–474.
[62] H. Zhu, Y. Wang, J. Xiao, M. Liu, S. Xiong, Z.J. Wong, Z. Ye, Y. Ye, X. Yin, X. Zhang, Nat. Nanotechnol. 10 (2014) 151.
[63] M.N. Blonsky, H.L. Zhuang, A.K. Singh, R.G. Hennig, ACS Nano 9 (2015) 9885–9891.
[64] C. Sevik, D. Çakır, O. Gülseren, F.M. Peeters, J. Phys. Chem. C 120 (2016) 13948–13953.
[65] W. Li, J. Li, Nano Res. 8 (2015) 3796–3802.
[66] T. Hu, J. Dong, Phys. Chem. Chem. Phys. 18 (2016) 32514–32520.
[67] R. Gao, Y. Gao, Phys. Status Solidi RRL 11 (2017) 1600412.
[68] G. Cheon, K.-A.N. Duerloo, A.D. Sendek, C. Porter, Y. Chen, E.J. Reed, Nano Lett. 17 (2017) 1915–1923.
[69] G. da Cunha Rodrigues, P. Zelenovskiy, K. Romanyuk, S. Luchkin, Y. Kopelevich, A. Kholkin, Nat. Commun. 6 (2015) 7572.
[70] S. Chandratre, P. Sharma, Appl. Phys. Lett. 100 (2012), 023114.
[71] K.E. El-Kelany, P. Carbonnière, A. Erba, M. Rérat, J. Phys. Chem. C 119 (2015) 8966–8973.
[72] M.T. Ong, K.-A.N. Duerloo, E.J. Reed, J. Phys. Chem. C 117 (2013) 3615–3620.
[73] M.T. Ong, E.J. Reed, ACS Nano 6 (2012) 1387–1394.
[74] M. Lopez-Suarez, M. Pruneda, G. Abadal, R. Rurali, Nanotechnology 25 (2014) 175401.
[75] Y. Zhou, W. Liu, X. Huang, A. Zhang, Y. Zhang, Z.L. Wang, Nano Res 9 (2016) 800–807.
[76] J.A. Wilson, A.D. Yoffe, Adv. Phys. 18 (1969) 193–335.
[77] S. Yu, K. Eshun, H. Zhu, Q. Li, Sci. Rep. 5 (2015) 12854.
[78] M.V. Bollinger, K.W. Jacobsen, J.K. Nørskov, Phys. Rev. B 67 (2003), 085410.
[79] W. Liu, A. Zhang, Y. Zhang, Z.L. Wang, Appl. Phys. Lett. 107 (2015) 083105.
[80] W. Liu, Y. Zhou, A. Zhang, Y. Zhang, Z.L. Wang, Appl. Phys. Lett. 108 (2016) 181603.
[81] D.Q. Zheng, Z. Zhao, R. Huang, J. Nie, L. Li, Y. Zhang, Nano Energy 32 (2017) 448–453.
[82] H. Yu, M. Liao, W. Zhao, G. Liu, X.J. Zhou, Z. Wei, X. Xu, K. Liu, Z. Hu, K. Deng, S. Zhou, J.-A. Shi, L. Gu, C. Shen, T. Zhang, L. Du, L. Xie, J. Zhu, W. Chen, R. Yang, D. Shi, G. Zhang, ACS Nano 11 (2017) 12001–12007.
[83] Z.L. Wang, Mater. Today 20 (2017) 74–82.
[84] S.K. Kim, R. Bhatia, T.-H. Kim, D. Seol, J.H. Kim, H. Kim, W. Seung, Y. Kim, Y.H. Lee, S.-W. Kim, Nano Energy 22 (2016) 483–489.
[85] P. Lin, Y. Gu, X. Yan, S. Lu, Z. Zhang, Y. Zhang, Nano Res 9 (2016) 1091–1100.
[86] S.A. Han, T.-H. Kim, S.K. Kim, K.H. Lee, H.-J. Park, J.-H. Lee, S.-W. Kim, Adv. Mater. 30 (2018) 1800342.
[87] J.-H. Lee, J.Y. Park, E.B. Cho, T.Y. Kim, S.A. Han, T.-H. Kim, Y. Liu, S.K. Kim, C.J. Roh, H.-J. Yoon, H. Ryu, W. Seung, J.S. Lee, J. Lee, S.-W. Kim, Adv. Mater. 29 (2017) 1606667.
[88] Y. Li, Y. Rao, K.F. Mak, Y. You, S. Wang, C.R. Dean, T.F. Heinz, Nano Lett. 13 (2013) 3329–3333.
[89] W.-T. Hsu, Z.-A. Zhao, L.-J. Li, C.-H. Chen, M.-H. Chiu, P.-S. Chang, Y.-C. Chou, W.-H. Chang, ACS Nano 8 (2014) 2951–2958.
[90] A.A. Puretzky, L. Liang, X. Li, K. Xiao, B.G. Sumpter, V. Meunier, D.B. Geohegan, ACS Nano 10 (2016) 2736–2744.
[91] X. Wang, Am. Ceram. Soc. Bull. 92 (2013) 18–23.
[92] M. Huang, T.A. Pascal, H. Kim, W.A. Goddard, J.R. Greer, Nano Lett. 11 (2011) 1241–1246.
[93] S. Manzeli, A. Allain, A. Ghadimi, A. Kis, Nano Lett. 15 (2015) 5330–5335.
[94] J. Qi, Y.-W. Lan, A.Z. Stieg, J.-H. Chen, Y.-L. Zhong, L.-J. Li, C.-D. Chen, Y. Zhang, K.L. Wang, Nat. Commun. 6 (2015) 7430.
[95] C. Pan, R. Yu, S. Niu, G. Zhu, Z.L. Wang, ACS Nano 7 (2013) 1803–1810.
[96] S. Niu, Y. Hu, X. Wen, Y. Zhou, F. Zhang, L. Lin, S. Wang, Z.L. Wang, Adv. Mater. 25 (2013) 3701–3706.
[97] G. Hu, R. Zhou, R. Yu, L. Dong, C. Pan, Z.L. Wang, Nano Res. 7 (2014) 1083–1091.
[98] R. Zhou, G. Hu, R. Yu, C. Pan, Z.L. Wang, Nano Energy 12 (2015) 588–596.
[99] J. Zhao, N. Li, H. Yu, Z. Wei, M. Liao, P. Chen, S. Wang, D. Shi, Q. Sun, G. Zhang, Adv. Mater. 29 (2017) 1702076.
[100] D.J. Late, Y.-K. Huang, B. Liu, J. Acharya, S.N. Shirodkar, J. Luo, A. Yan, D. Charles, U.V. Waghmare, V.P. Dravid, C.N.R. Rao, ACS Nano 7 (2013) 4879–4891.
[101] F.K. Perkins, A.L. Friedman, E. Cobas, P.M. Campbell, G.G. Jernigan, B.T. Jonker, Nano Lett. 13 (2013) 668–673.
[102] J. Guo, R. Wen, Y. Liu, K. Zhang, J. Kou, J. Zhai, Z.L. Wang, ACS Appl. Mater. Interfaces 10 (2018) 8110–8116.
[103] G. Hu, R. Zhou, R. Yu, L. Dong, C. Pan, Z.L. Wang, Nano Res 7 (2014) 1083–1091.
[104] C. Xie, C. Mak, X. Tao, F. Yan, Adv. Funct. Mater. 27 (2016) 1603886.
[105] X. Duan, C. Wang, A. Pan, R. Yu, X. Duan, Chem. Soc. Rev. 44 (2015) 8859–8876.
[106] K.F. Mak, J. Shan, Nat. Photonics 10 (2016) 216–226.
[107] S. Parui, L. Pietrobon, D. Ciudad, S. Vélez, X. Sun, F. Casanova, P. Stoliar, L.E. Hueso, Adv. Funct. Mater. 25 (2015) 2972–2979.
[108] D. Jariwala, S.L. Howell, K.-S. Chen, J. Kang, V.K. Sangwan, S.A. Filippone, R. Turrisi, T.J. Marks, L.J. Lauhon, M.C. Hersam, Nano Lett. 16 (2016) 497–503.
[109] W. Wu, L. Wang, R. Yu, Y. Liu, S.-H. Wei, J. Hone, Z.L. Wang, Adv. Mater. 28 (2016) 8463–8468.
[110] O. Lopez-Sanchez, D. Lembke, M. Kayci, A. Radenovic, A. Kis, Nat. Nanotechnol. 8 (2013) 497–501.
[111] K. Zhang, M. Peng, W. Wu, J. Guo, G. Gao, Y. Liu, J. Kou, R. Wen, Y. Lei, A. Yu, Y. Zhang, J. Zhai, Z.L. Wang, Mater. Horiz. 4 (2017) 274–280.
[112] M.S. Choi, D. Qu, D. Lee, X. Liu, K. Watanabe, T. Taniguchi, W.J. Yoo, ACS Nano 8 (2014) 9332–9340.
[113] Y. Zhao, K. Xu, F. Pan, C. Zhou, F. Zhou, Y. Chai, Adv. Funct. Mater. 27 (2016) 1603484.
[114] K. Zhang, J. Zhai, Z.L. Wang, 2D Mater. 5 (2018), 035038.
[115] P. Lin, L. Zhu, D. Li, L. Xu, C. Pan, Z. Wang, Adv. Funct. Mater. 28 (2018) 1802849.

[116] C. Cui, F. Xue, W.-J. Hu, L.-J. Li, npj 2D Mater. Appl. 2 (2018), https://doi.org/10.1038/s41699-018-0063-5.

[117] Y. Peng, M. Que, J. Tao, X. Wang, J. Lu, G. Hu, B. Wan, Q. Xu, C. Pan, 2D Mater. 5 (2018), 042003.

[118] G. Gao, B. Wan, X. Liu, Q. Sun, X. Yang, L. Wang, C. Pan, Z.L. Wang, Adv. Mater. 30 (2018) 1705088.

[119] M.-Y. Li, Y. Shi, C.-C. Cheng, L.-S. Lu, Y.-C. Lin, H.-L. Tang, M.-L. Tsai, C.-W. Chu, K.-H. Wei, J.-H. He, W.-H. Chang, K. Suenaga, L.-J. Li, Science 349 (2015) 524–528.

[120] M.-Y. Li, C.-H. Chen, Y. Shi, L.-J. Li, Mater. Today 19 (2016) 322–335.

[121] Y. Son, M.-Y. Li, C.-C. Cheng, K.-H. Wei, P. Liu, Q.H. Wang, L.-J. Li, M.S. Strano, Nano Lett. 16 (2016) 3571–3577.

[122] A.K. Geim, I.V. Grigorieva, Nature 499 (2013) 419–425.

[123] F. Xue, L. Chen, J. Chen, J. Liu, L. Wang, M. Chen, Y. Pang, X. Yang, G. Gao, J. Zhai, Z.L. Wang, Adv. Mater. 28 (2016) 3391–3398.

[124] X. Yu, T.J. Marks, A. Facchetti, Nat. Mater. 15 (2016) 383–396.

[125] X. Gong, O. Voznyy, A. Jain, W. Liu, R. Sabatini, Z. Piontkowski, G. Walters, G. Bappi, S. Nokhrin, O. Bushuyev, M. Yuan, R. Comin, D. McCamant, S.O. Kelley, E.H. Sargent, Nat. Mater. 17 (2018) 550–556.

[126] J. Hu, L. Yan, W. You, Adv. Mater. (2018) 1802041, https://doi.org/10.1002/adma.201802041.

[127] F. Yang, S. Cheng, X. Zhang, X. Ren, R. Li, H. Dong, W. Hu, Adv. Mater. 30 (2017) 1702415.

[128] S.K. Park, J.H. Kim, S.Y. Park, Adv. Mater. 30 (2018) 1704759.

[129] R.R.Q. Freitas, R. Rivelino, F. de Brito Mota, C.M.C. de Castilho, A. Kakanakova-Georgieva, G.K. Gueorguiev, J. Phys. Chem. C 119 (2015) 23599–23606.

[130] L. Kou, Y. Ma, Z. Sun, T. Heine, C. Chen, J. Phys. Chem. Lett. 8 (2017) 1905–1919.

[131] C. Gong, L. Li, Z. Li, H. Ji, A. Stern, Y. Xia, T. Cao, W. Bao, C. Wang, Y. Wang, Z.Q. Qiu, R.J. Cava, S.G. Louie, J. Xia, X. Zhang, Nature 546 (2017) 265–269.

[132] X. Qian, J. Liu, L. Fu, J. Li, Science 346 (2014) 1344–1347.

[133] Y. Zhang, Y. Yang, Y. Gu, X. Yan, Q. Liao, P. Li, Z. Zhang, Z. Wang, Nano Energy 14 (2015) 30–48.